Transport coefficients of the Lennard-Jones model fluid. III. Bulk viscosity

Karsten Meier[a)]
Institut für Thermodynamik, Helmut-Schmidt-Universität—Universität der Bundeswehr Hamburg, Holstenhofweg 85, D-22043 Hamburg, Germany

Arno Laesecke
Physical and Chemical Properties Division, Chemical Science and Technology Laboratory, National Institute of Standards and Technology, Boulder, Colorado 80305

Stephan Kabelac
Institut für Thermodynamik, Helmut-Schmidt-Universität—Universität der Bundeswehr Hamburg, Holstenhofweg 85, D-22043 Hamburg, Germany

(Received 4 August 2004; accepted 11 October 2004; published online 15 December 2004)

In an extensive computer simulation study, the transport coefficients of the Lennard-Jones model fluid were determined with high accuracy from equilibrium molecular-dynamics simulations. In the frame of time-correlation function theory, the generalized Einstein relations were employed to evaluate the transport coefficients. This third of a series of four papers presents the results for the bulk viscosity. With comprehensive simulation data at over 350 state points, the temperature and density dependences of the bulk viscosity are characterized in this work over a wide range of fluid states. The bulk viscosity exhibits a large critical enhancement similar to that known for the thermal conductivity, but it extends much farther into the supercritical region and can be observed even at 4.5 times the critical temperature. An investigation of the pressure-fluctuation autocorrelation functions shows that the enhancement is caused by extremely slowly decaying pressure fluctuations. © *2005 American Institute of Physics.* [DOI: 10.1063/1.1828040]

I. INTRODUCTION

This is the third of a series of four papers in which the results of an extensive molecular-dynamics simulation study on the transport coefficients of the Lennard-Jones model fluid[1,2] are reported. It presents the results for the bulk viscosity. The results for the viscosity and self-diffusion coefficient have been discussed in two preceding papers[3,4] referred to hereafter as Papers I and II, and a subsequent paper deals with the thermodynamic properties.[5]

The hydrodynamic transport coefficient bulk viscosity η_b relates the difference between the nonequilibrium pressure p^{ne} and thermodynamic equilibrium pressure p^{eq} to the divergence of the velocity field $\mathbf{v}$ by the constitutive equation[6]

$$p^{\mathrm{ne}} - p^{\mathrm{eq}} = -\eta_b \nabla \cdot \mathbf{v}. \tag{1}$$

It describes viscous effects associated with the change of volume of an infinitesimal volume element of a fluid at constant shape of the volume element, while viscous effects associated with changes of shape at constant volume are described by the viscosity η. Sometimes, the bulk viscosity is termed volume viscosity or dilatation viscosity in the literature. Very little is known about this transport coefficient. In fluid mechanics, bulk viscosity effects are often neglected. This is correct if the fluid is an ideal monatomic gas, or if it is treated as an incompressible fluid. In these cases, the bulk viscosity is exactly zero.[6] However, in some applications, such as the spread of shock wave fronts or the attenuation of sound waves, dilatation and compression of the fluid are important effects, and therefore knowledge of the bulk viscosity is required in these applications.

Experimental bulk viscosity data are available for a few fluids, but are often restricted to a limited set of state points. Reviews of experimental data are given by Hanley and Cohen[7] and in the survey paper of Graves and Argrow.[8] Presently, comprehensive data sets characterizing the bulk viscosity of a fluid over a wide range of density and temperature are not available.

Bulk viscosities are usually determined from experimental data of the sound absorption coefficient α, which in classical acoustics is given by

$$\frac{\alpha}{f^2} = \frac{2\pi^2}{\rho_m w_0^3}\left[\frac{c_{p,m} - c_{v,m}}{c_{p,m} c_{v,m}}\lambda + \frac{4}{3}\eta + \eta_b\right]. \tag{2}$$

Here, f denotes the frequency, w_0 is the zero-frequency speed of sound, λ is the thermal conductivity, and ρ_m, $c_{p,m}$, and $c_{v,m}$ stand, respectively, for the mass density, specific isobaric heat capacity, and specific isochoric heat capacity. Equation (2) shows that the specific isochoric and isobaric heat capacity, zero-frequency speed of sound, thermal conductivity, and viscosity must be known accurately at the state point of the measurement to obtain a precise value for the bulk viscosity. As such data sets are rarely available, experimental bulk viscosity data are often associated with large uncertainties.

[a)]Electronic mail: karsten.meier@hsuhh.de

On the other hand, bulk viscosities can be determined with little additional computational effort together with the viscosity in molecular-dynamics simulations. Therefore, bulk viscosity data for the Lennard-Jones model fluid were derived in this work from the same simulations from which the viscosity data and self-diffusion coefficients reported in Papers I and II were obtained. With these data, the temperature and density dependences of the bulk viscosity are characterized over a large part of the fluid region.

This paper is organized as follows: The following section provides the theoretical background for the calculation of the bulk viscosity in equilibrium molecular-dynamics simulations, and describes the simulation procedure and analysis of the results. Section III presents an investigation of the influence of simulation parameters on the results for the bulk viscosity. In Sec. IV, the bulk viscosity data are discussed and compared with literature data of other research groups. In Sec. V, the dependence of the bulk viscosity on density and temperature is examined. Finally, an investigation of the pressure-fluctuation autocorrelation functions in Sec. VI provides an interpretation of the behavior of the bulk viscosity in the fluid region.

II. SIMULATION PROCEDURE

There are two different approaches to calculate the bulk viscosity by molecular-dynamics simulations: either by nonequilibrium molecular dynamics or by time-correlation function theory employing the Green-Kubo integral formula or the Einstein relation in equilibrium simulations. For reasons presented in Paper I, equilibrium molecular-dynamics simulations were chosen, and time-correlation function theory was used to determine the transport coefficients of the Lennard-Jones model fluid.

In time-correlation function theory, the bulk viscosity η_b is given by the Green-Kubo integral formula[9]

$$\eta_b = \frac{V}{kT}\int_0^\infty \langle \delta p(t)\ \delta p(t_0)\rangle dt, \tag{3}$$

or, equivalently, by the Einstein relation[10]

$$\eta_b = \lim_{t\to\infty} \frac{V}{kT}\frac{d}{dt}\left\langle \left[\frac{m}{3V}\sum_{i=1}^{N} \left[\mathbf{v}_i(t)\cdot\mathbf{r}_i(t) - \mathbf{v}_i(t_0)\cdot\mathbf{r}_i(t_0)\right] - \langle p\rangle (t-t_0)\right]^2 \right\rangle. \tag{4}$$

In these equations, V denotes the volume, k is the Boltzmann constant, T stands for the temperature, t is time, and $\delta p = p - \langle p\rangle$ is termed pressure fluctuation. It is the instantaneous deviation of the pressure p from the average pressure $\langle p\rangle$. N is the number of particles, and $\mathbf{r}_i$ and $\mathbf{v}_i$ are the position and velocity vectors of particle i. The angular brackets in Eqs. (3) and (4) indicate equilibrium ensemble averages over short trajectory sections of the phase-space trajectory of the system with time origins t_0. The instantaneous pressure is given by[11]

$$p = \frac{1}{3V}\left(\sum_{i=1}^{N} m\mathbf{v}_i^2 + \sum_{i=1}^{N-1}\sum_{j=i+1}^{N} \mathbf{r}_{ij}\cdot\mathbf{F}_{ij}\right), \tag{5}$$

where m denotes the particle mass, $\mathbf{r}_{ij} = \mathbf{r}_i - \mathbf{r}_j$, and $\mathbf{F}_{ij}$ is the force of particle i acting on particle j, and the average pressure is the simulation average of the instantaneous pressure.

The Green-Kubo integral formula determines the bulk viscosity as the integral of the pressure-fluctuation autocorrelation function, whereas the Einstein relation relates it to the slope of a generalized mean-squared displacement function in the long-time limit $t\to\infty$. From a mathematical point of view, both the Green-Kubo integral formula, Eq. (3), and the Einstein relation, Eq. (4), are completely equivalent[9] and could in principle be used to determine the bulk viscosity. In this work, the Einstein relation method was chosen.

As discussed in Paper I for the viscosity, the Einstein relation for the bulk viscosity cannot be directly applied in molecular-dynamics simulations because the generalized displacement function is a discontinuous function of time. It has to be replaced by the time integral of the pressure fluctuation:

$$\int_{t_0}^{t} \delta p(t)dt = \frac{m}{3V}\sum_{i=1}^{N} \left[\mathbf{v}_i(t)\cdot\mathbf{r}_i(t) - \mathbf{v}_i(t_0)\cdot\mathbf{r}_i(t_0)\right] - \langle p\rangle (t-t_0). \tag{6}$$

Equation (6) is obtained by an integration by parts of the pressure fluctuation $\delta p = p - \langle p\rangle$, with the molecular expression for the pressure, Eq. (5), inserted. The modified Einstein relation reads

$$\eta_b = \frac{V}{2kT}\lim_{t\to\infty}\frac{d}{dt}\left\langle \left[\int_0^t \delta p(t)dt\right]^2\right\rangle. \tag{7}$$

As the molecular expression for the pressure is a function of the distances between all pairs of particles, the time evolution of the pressure fluctuation is continuous if periodic boundary conditions and the minimum-image convention are applied. Therefore, Eq. (7) provides an indirect way to evaluate the bulk viscosity by its Einstein relation in equilibrium molecular-dynamics simulations.

The bulk viscosity data were derived from the same simulations from which the viscosity data and self-diffusion coefficients reported in Papers I and II were obtained. All simulations were carried out in the classical molecular-dynamics ensemble at constant NVE**MG**, as described in Paper I. At every simulated time step, the instantaneous properties of the system are calculated and stored. After a simulation run, several separate analysis programs were used to compute thermodynamic state variables, time-correlation functions, and generalized mean-squared displacement functions from the stored data. In a subsequent analysis step, the bulk viscosity data were obtained from a careful analysis of the Einstein relations and pressure fluctuation autocorrelation functions by the same procedure as described in Paper I for the viscosity.

In the remainder of this paper, reduced quantities denoted by a superscript asterisk "*" are used, e.g., $T^* = Tk/\varepsilon$, $\rho^* = \rho\sigma^3$, $t^* = t\sqrt{\varepsilon/m}/\sigma$, $r^* = r/\sigma$, $\mathbf{v}^* = \mathbf{v}\sqrt{m/\varepsilon}$, and $\eta_b^* = \eta_b\sigma^2/\sqrt{m\varepsilon}$, where ε and σ are the energy and length scaling parameters of the Lennard-Jones potential.

TABLE I. Simulation data for the bulk viscosity near the state point ($T^*=0.722$, $\rho^*=0.8442$) close to the triple point of the Lennard-Jones model fluid.

N	r_{cut}^*	T^*	η_b^*
108	2.5	0.731 262	1.290
256	3.25	0.733 052	1.185
500	4.0	0.722 001	1.102
864	5.0	0.721 355	1.139
2048	5.5	0.721 444	1.217
4000	5.5	0.722 109	1.194
4000	5.5	0.722 096	1.145[a]
1372	2.5	0.723 441	1.186
1372	2.75	0.732 155	1.092
1372	3.0	0.712 572	1.123
1372	3.25	0.730 478	1.196
1372	3.5	0.717 710	1.163
1372	3.75	0.719 279	1.147
1372	4.0	0.721 561	1.163
1372	4.25	0.718 948	1.137
1372	4.5	0.721 795	1.159
1372	4.75	0.721 195	1.153
1372	5.0	0.721 228	1.140
1372	5.25	0.722 564	1.148
1372	5.5	0.722 266	1.133

[a]25×10^6 time steps.

III. INFLUENCE OF SIMULATION PARAMETERS ON THE BULK VISCOSITY

Any simulation result is subject to statistical and systematic errors. Statistical errors were estimated by the method described by Allen and Tildesley,[11] which is originally due to Friedberg and Cameron.[12]

Systematic errors can be eliminated to some extent by a careful choice of the simulation parameters. Since it is not *a priori* known how the simulation parameters, e.g., cutoff radius or number of particles, must be chosen, a systematic investigation of their influence on the results for macroscopic properties is required.

The influence of the number of particles N and the cutoff radius on the bulk viscosity was investigated at the state point ($T^*=0.722$, $\rho^*=0.8442$) close to the triple point, at which the influence of these parameters on the viscosity was already examined in paper I. The results of these simulations are reported in Table I. As this state point was the subject of many simulation studies, a few literature data for the bulk viscosity are available.[13–19]

The influence of the number of particles was examined by seven simulations with 108–4000 particles extending over 10 million time steps each. In simulations with 1372 or more particles, the cutoff radius was set to $r_{cut}^*=5.5$, while in simulations with fewer particles it was chosen slightly smaller than half the box length. After 10×10^6 time steps, the simulation with 4000 particles was continued up to 25×10^6 time steps.

Figure 1 shows the bulk viscosity data together with literature data as a function of the inverse number of particles. The present results are more consistent than the literature data. Good agreement is found between the present data and the two data $\eta_b^*=1.14$ and 1.20 reported by Levesque and Verlet for 864 particles,[13] with the datum $\eta_b^*=1.16$ of Hoheisel, Vogelsang, and Schoen[14] for 256 particles, and with the datum $\eta_b^*=1.14$ published by Schoen[15] for 500 particles. The datum $\eta_b^*=1.05$ of Levesque, Verlet, and Kürkijarvi[16] and other data $\eta_b^*=1.13$, 0.89, and 1.04 of Levesque and Verlet[13] obtained with 108, 256, and 864 particles are lower than the present data. The data of Hoover *et al.*[17] and Heyes[18,19] $\eta_b^*=1.55$ and $\eta_b^*=1.47$ are much higher than all other data and lie outside the range of Fig. 1. This large difference may be due to the use of nonequilibrium simulations in these studies. The datum of Hoheisel[20] $\eta_b^*=1.17$ was obtained at the higher temperature $T^*=0.78$ and can therefore not be compared directly with the other data.

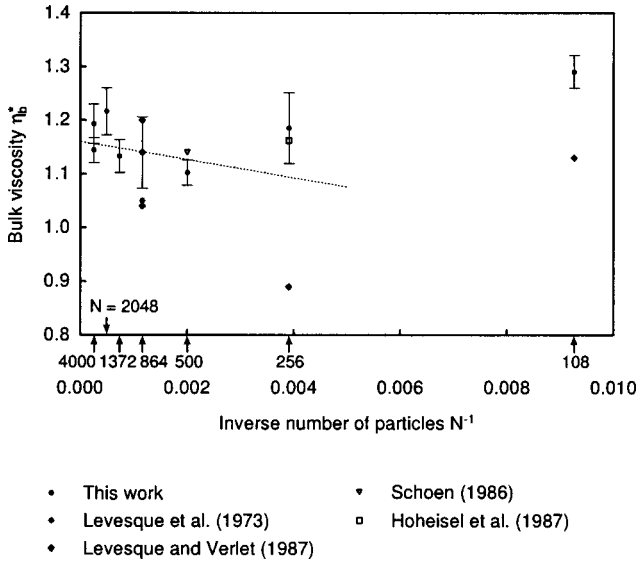

FIG. 1. Present simulation data and literature data for the bulk viscosity η_b^* at the state point ($T^*=0.722$, $\rho^*=0.8442$) as a function of the inverse number of particles. Error bars designate the uncertainty of the present data, and the dashed line represents a weighted linear-least-squares fit to the present data.

As for the viscosity in Paper I, an estimate for the bulk viscosity for the infinite system size limit was derived from a weighted linear-least-squares fit to the present data, yielding

$$\eta_b^*=1.161\pm0.019.$$

As it was found in Paper I that the viscosity increases with the number of particles, it is reasonable to assume that the bulk viscosity shows the same behavior. If the value for 108 particles is included in the fit, the fitted straight line will decrease with the number of particles. For this reason, and because the value for 108 particles appears to be too high compared with the other data, it was excluded from the fit.

To conclude, for the target system size of 1372 particles employed in the present simulations the statistical uncertainty of the data is larger than their dependence on the number of particles, even for long simulation runs over 10×10^6 time steps. Therefore, the dependence of the bulk viscosity data on the number of particles is negligible. An exception is the region near the critical point, where correlations decay extremely slowly. In this region, the results for the bulk viscosity are expected to depend significantly on the number of particles. However, the influence of the number of particles in this state region was not investigated.

TABLE II. Data sets for the bulk viscosity of the Lennard-Jones model fluid. Included are data at the state point ($T^*=0.722$, $\rho^*=0.8442$) close to the triple point, which are discussed in Sec. III. Abbreviations: DT, difference in trajectories method; ER, Einstein relation; GK, Green-Kubo integrals; OS, oscillating strain perturbed Hamiltonian method; and TS, trajectory segments.

Author	Year	Data	Method	Ensemble	N	r_{cut}^*	T^*	ρ^*	Simulation length[a]
This work	2005	344	ER	*NVE***MG**	1372	5.5–6.5	0.7–6.0	0.005–1.275	4500–6000
This work	2005	39	ER	*NVE***MG**	1372	6.5	0.7–1.2	0.005–0.15	150 000
Borgelt[b], Ref. 23	1990	46	GK	*NVE***MG**	108	2.5	0.66–2.93	0.78–0.883	371
Canales[c], Ref. 24	1999	3	GK/ER	*NVT*	668	2.71–3.11	0.53–1.893	0.756, 1.143	550–1200
Heyes[d], Ref. 18	1984	39	DT	⋯	256	2.5	0.71–4.56	0.5–1.05	180 TS
Heyes[e], Ref. 25	1993	4	GK	*NVE***MG**	256	2.5	0.7–6.0	0.5–1.0	655–17100
Hoheisel[f], Ref. 20	1987	4	GK	*NVE***MG**	256	1.5–3.2	0.78	0.8442	230, 460
Hoheisel[g], Ref. 14	1987	11	GK	*NVE***MG**	256	2.5	0.68–2.58	0.42–1.04	464–1856
Hoover[h], Ref. 17	1980	1	OS	⋯	54	[b]	0.722	0.8442	126–5027
Levesque[j], Ref. 16	1973	1	GK	*NVE***MG**	864	2.5	0.722	0.8442	465.6
Levesque[k], Ref. 13	1987	9	GK	*NVE***MG**	108–864	[b]	0.715–2.8	0.8442–1.113	11.04–88.32
Schoen[l], Ref. 15	1986	1	GK	*NVE***MG**	500	2.5	0.73	0.8442	464

[a]Values of the simulation length are given in reduced time units.
[b]Not reported by the authors.

The influence of the cutoff radius on the simulation results was investigated at the same state point ($T^*=0.722$, $\rho^*=0.8442$). Above $r_{cut}^*=4.5$ these simulation data show no dependence on the cutoff radius. Evidently, the influence of the cutoff radius is negligible if it is chosen larger than 4.5.

IV. RESULTS FOR THE BULK VISCOSITY

For the determination of the transport coefficients of the Lennard-Jones model fluid over a wide range of fluid states, extensive equilibrium molecular-dynamics simulations were carried out at 351 state points along 16 isotherms. The parameters for this main body of simulations and the distribution of the simulated state points in relation to the phase boundaries were described in paper I. The simulations extend over a wide range of the fluid region from the low-density gas to the compressed liquid close to the freezing line and cover the temperature range between $T^*=0.7-6.0$. At every simulated state point, several thermodynamic properties and the transport coefficients viscosity, bulk viscosity, and the self-diffusion coefficient were evaluated. While this paper discusses the bulk viscosity, the results for the viscosity and self-diffusion coefficient were reported in Papers I and II, and a subsequent paper will discuss the results for the thermodynamic properties.

In addition to this large body of simulations, two further simulation series were carried out. One series repeated simulations at low-temperature gaseous states between the temperatures $T^*=0.7$ and 1.2 on 39 state points. The production phases of these simulations extended over 50×10^6 time steps. These simulations were performed to determine the behavior of the viscosity and bulk viscosity in this state region more precisely. Another 11 simulations extending over 10×10^6 time steps were performed mainly, on the near-critical isotherm $T^*=1.35$, to determine the behavior of the bulk viscosity and thermal conductivity in the vicinity of the critical point more precisely.

At every simulated state point, generalized mean-squared displacement functions and pressure-fluctuation autocorrelation functions were computed. The instantaneous values of the pressure were stored at every time step during the production phase of the simulation. Time origins were taken at every fifth time step. The bulk viscosities were determined from the modified Einstein relation, Eq. (7). The simulation data of this work were deposited as text files in the electronic archive of this paper[21] and in the electronic archive of the NIST Physical and Chemical Properties Division.[22] The statistical uncertainty of the data is estimated to be 5% in the liquid at high densities above $\rho^*=0.3$. At lower densities and in the vicinity of the critical point, the uncertainty is higher, amounting up to 30%. The low-temperature gas data of the second series of extremely long simulations over 50 million time steps have uncertainties of 10%, but increasing up to 20% at the lowest densities.

Nine literature sources report simulation data for the bulk viscosity of the Lennard-Jones model fluid. The details of the present data and these data sets are summarized in Table II. Only in three sources, the works of Heyes,[18] Hoheisel, Vogelsang, and Schoen;[14] and of Borgelt, Hoheisel, and Stell,[23] data at more than ten state points are reported. In a further paper, Heyes[19] reported simulations at 45 states, from which 36 states coincide with those of Ref. 18. Unfortunately, the bulk viscosity data were not reported in the publication. Instead, the data were regressed and the parameters of the resulting equation were published. With only few exceptions, the literature data were derived from simulations with less than 500 molecules. In most literature studies, the cutoff radius was set to $r_{cut}^*=2.5$. Furthermore, the production phases of the literature simulations are in most cases much shorter than those of the present simulations.

The distribution of the state points of the three largest literature data sets in the fluid region is shown in Fig. 2 in the T^*, ρ^* plane. The data of Borgelt, Hoheisel, and Stell[23] are distributed along three isochors in the liquid region and extend up to the temperature $T^*=3.0$. The data set of Heyes[18] covers a larger density range and extends up to $T^*=4.5$. The 11 data of Hoheisel, Vogelsang, and Schoen[14] are provided at states close to state points simulated by Heyes.[18] These data sets focus on the liquid region. The simulations of this work cover a much larger part of the fluid region, including the

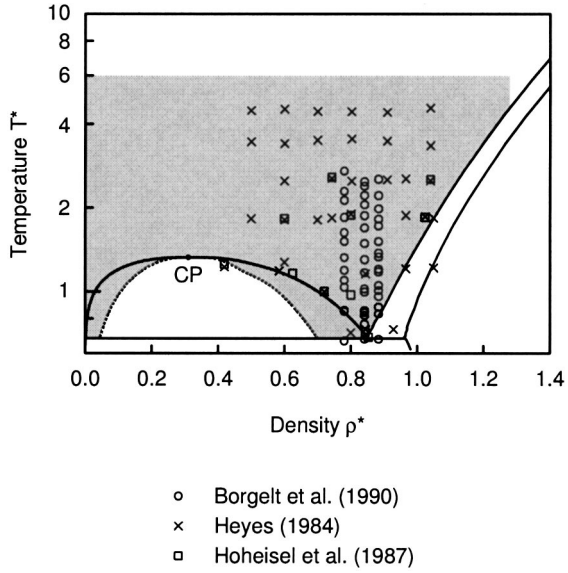

FIG. 2. The distribution of literature data for the bulk viscosity η_b^* in the T^*,ρ^* plane. The shaded area is the state region investigated in this work.

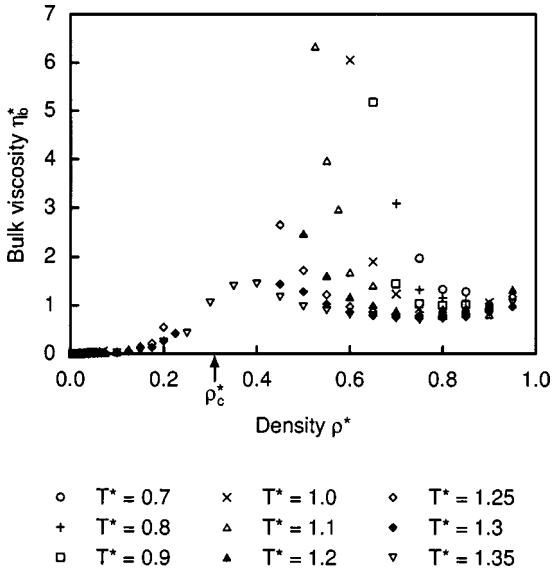

FIG. 4. The bulk viscosity for all simulated subcritical isotherms as a function of density. For stability limits, see Fig. 2.

vicinity of the critical density at supercritical temperatures and the low density gas region.

Figure 3 shows the isochoric data of Borgelt, Hoheisel, and Stell[23] at the densities $\rho^*=0.7801$, $\rho^*=0.8415$, and $\rho^*=0.8836$ and data of this work along the three closest isochors $\rho^*=0.8$, $\rho^*=0.85$, and $\rho^*=0.9$. At the displayed liquid densities, the bulk viscosity decreases steeply at subcritical temperatures, but shows little temperature dependence at supercritical temperatures. The data of this work give a consistent picture for the three isochors, whereas the data of Borgelt, Hoheisel, and Stell show large scatter, so that the individual isochors cannot be distinguished. The temperature dependence of both data sets is similar.

A comprehensive comparison with the data of Heyes[18] is difficult to perform because there are only a few state points which coincide with states of the present simulations. For example, Heyes reports $\eta_b^*=1.05$ for the state ($T^*=1.81$, $\rho^*=0.6$) and $\eta_b^*=0.77$ for the ($T^*=2.5$, $\rho^*=0.7$). The results of this work at ($T^*=1.8$, $\rho^*=0.6$) and ($T^*=2.5$, $\rho^*=0.7$) are $\eta_b^*=0.5861$ and $\eta_b^*=0.5835$, respectively. The magnitude of the difference between the data is similar to that observed at the previously discussed state point close to the triple point. Therefore, the discrepancy appears to be due to the different simulation methods used.

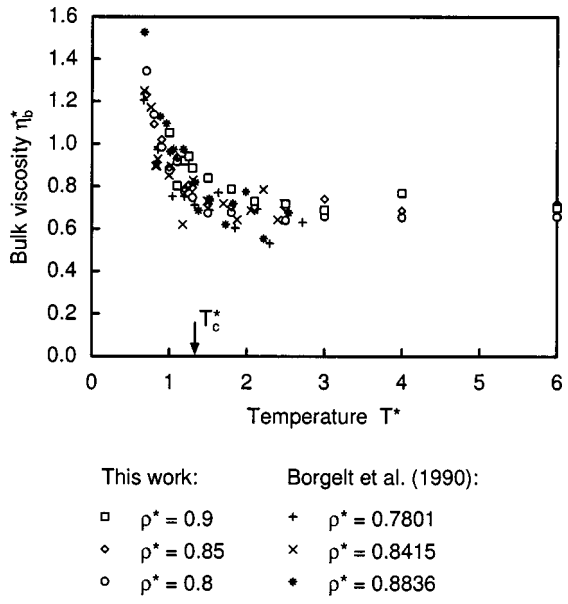

FIG. 3. Bulk viscosity data along isochors at high densities.

The data of Hoheisel, Vogelsang, and Schoen[14] are also difficult to compare with the present data. At ($T^*=1.833$, $\rho^*=0.6$) and ($T^*=2.533$, $\rho^*=1.040$) they report $\eta_b^*=0.542$ and $\eta_b^*=0.908$, while the present results at ($T^*=1.8$, $\rho^*=0.6$) and ($T^*=2.5$, $\rho^*=1.05$) are $\eta_b^*=0.5861$ and $\eta_b^*=1.024$. Hoheisel, Vogelsang, and Schoen pointed out that their data at the highest densities are too small by about 10%. If additionally the simulation parameters of their simulations are compared with those of the present simulations (see Table II), the agreement of the data is satisfactory.

The comparison with the literature data shows that the present results are far more accurate and much wider ranging than any previously published data for the bulk viscosity of the Lennard-Jones model fluid.

V. TEMPERATURE AND DENSITY DEPENDENCE OF THE BULK VISCOSITY

With the present simulation data, the behavior of the bulk viscosity is characterized in the fluid region. Figure 4 displays the results for gas and liquid subcritical isotherms, and Fig. 5 presents the gas data of the second simulation series. In the zero-density limit, the bulk viscosity is zero since the Lennard-Jones model fluid is a monatomic fluid.[6] Close to the zero-density limit, the isotherms are flat, but increase more strongly as they enter the metastable region. When the isotherms approach the stability limit in the metastable region (for stability limits see Fig. 2), they diverge. The low-temperature liquid isotherms increase monotoni-

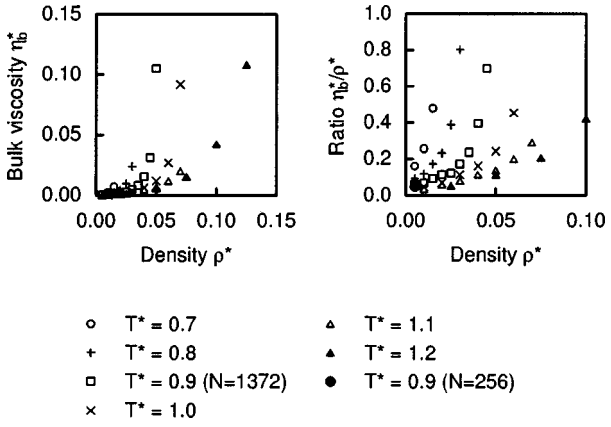

FIG. 5. The bulk viscosity and the ratio of bulk viscosity and density at gaseous states on subcritical isotherms as a function of density.

cally with decreasing density. At higher, but still subcritical temperatures, the liquid isotherms decrease close to the freezing line, exhibit minima, and then increase strongly when entering the metastable region. As the gas isotherms, the liquid isotherms diverge in the metastable region when they approach the stability limit.

Figure 6 depicts the data on supercritical isotherms. The behavior observed for subcritical isotherms continues into the supercritical region. The near-critical isotherm $T^*=1.35$ increases in the gas region, exhibits a maximum close to the critical density, decreases, and reaches a minimum before increasing towards the freezing line. In the vicinity of the critical density, the bulk viscosity shows a large enhancement. With increasing temperature, the enhancement becomes broader and smaller in magnitude. Moreover, it is shifted to higher densities. When the temperature is further increased, the maximum vanishes, and the isotherms increase monotonically. Nevertheless, the enhancement is still observed on the highest isotherm $T^*=6.0$ at about 4.5 times the critical temperature. This effect is similar to the enhancement of the thermal conductivity in the vicinity of the critical point, which is experimentally observed for real fluids.[26–28] In contrast to the critical enhancement of the thermal conductivity, the enhancement of the bulk viscosity is not restricted to a small region close to the critical point, but dominates the bulk viscosity over a far wider range of fluid states. It is expected that the enhancement becomes even larger when systems larger than those of this work are considered.

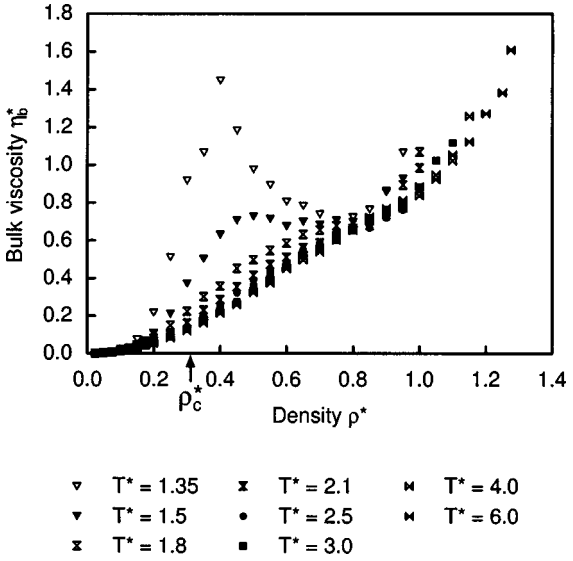

FIG. 6. The bulk viscosity for all simulated supercritical isotherms as a function of density.

As the bulk viscosity isotherms are very flat close to the zero-density limit, the question arises whether the initial slope, e.g., the second bulk viscosity virial coefficient $B^*_{\eta_b}$, is zero or wether it takes small positive nonzero values. Negative bulk viscosity virial coefficients are not allowed since the bulk viscosity is zero at zero density and it must always be positive at nonzero densities.[6] This issue can be examined by the same method used in Paper I to assess the initial slope of the potential-potential viscosity contribution isotherms. Figure 5 shows the ratio of the bulk viscosity and density for the gas data of the second simulation series. In this representation, the second bulk viscosity virial coefficient for a selected temperature is given by the intersection of the extrapolated isotherm with the ordinate. The isotherms between $T^*=0.7$ and 1.0 extrapolate to nonzero values in the zero-density limit, suggesting that the second bulk viscosity virial coefficient is nonzero. Moreover, $B^*_{\eta_b}$ takes the largest value at the lowest simulated temperature and decreases with temperature. For the two highest temperatures, the extrapolation is complicated by the fact that the effect is much weaker. At the isotherm $T^*=1.1$, the scatter of the data at the lowest densities is too large for an unambiguous extrapolation to zero density, and on the isotherm $T^*=1.2$ the data do not extend close enough to zero density.

The theory of the second transport virial coefficients as developed by Curtiss and co-workers[29] predicts that the bulk viscosity virial coefficient is identically zero. However, as for the second self-diffusion virial coefficient, this treatment of the second bulk viscosity virial coefficient lacks the improvements of the theory by Rainwater and Friend[30] and might therefore be in error.

The simulation results for the bulk viscosity of the Lennard-Jones model fluid can only be compared with experimental data only for monatomic fluids, e.g., noble gases, since internal degrees of freedom in molecular fluids yield contributions to the bulk viscosity that cannot be described by the simple Lennard-Jones potential. Experimental bulk viscosity data for argon are available at a few state points at moderate pressures.[31,32] The most comprehensive investigation is the work of Cowan and Ball,[31] who determined the bulk viscosity of liquid argon in the temperature range between $T=90$ and 150 K from the vapor pressure up to 7 MPa from measurements of the sound absorption coefficient.

Their results for nine isotherms are displayed in Fig. 7. The lowest isotherm is slightly higher than the triple point temperature of argon, $T_{tr}=83.8$ K, while the highest isotherm at 150 K is very close to the critical temperature $T_c=150.7$ K. The experimental data lie in a small density region close to the bubble line, whereas the present simulation data in the liquid region extend from the stability limit to the freezing line. At high temperatures, the qualitative behavior of the experimental and simulated isotherms is similar. They

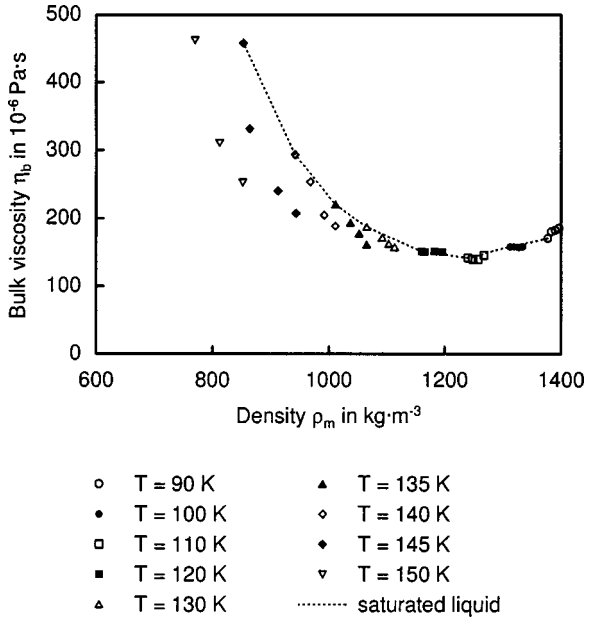

FIG. 7. The bulk viscosity of liquid argon as a function of density as measured by Cowan and Ball (Ref. 31). Critical parameters of argon: $T_c = 150.7$ K, $\rho_{m,c} = 530.9$ kg m^{-3}.

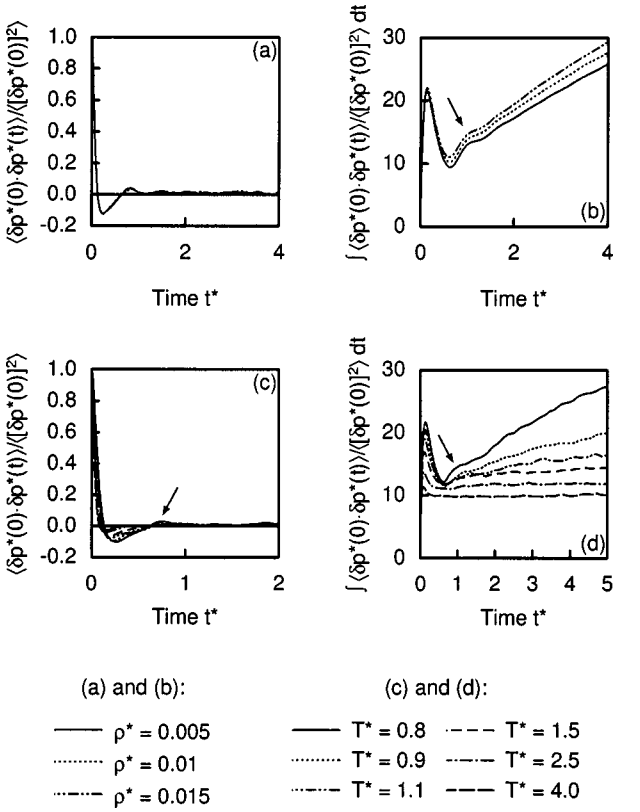

FIG. 8. Short-time behavior of the normalized pressure-fluctuation autocorrelation function and its time integral at gaseous densities. Note the different abscissa scale in the subfigures. The arrow points at special features of the correlation functions addressed in the text. (a) and (b) Density dependence on the lowest isotherm $T^* = 0.7$. (c) and (d). Temperature dependence along the isochor $\rho^* = 0.025$.

increase strongly as the bubble density is approached. Between $T = 100$ and 120 K, the bulk viscosity of argon is almost constant close to the bubble line. The constant part of the isotherms is also found for the simulation data in the range of the minima. On the lowest isotherm, $T = 90$ K, close to the triple point, the bulk viscosity increases with density. The simulation data on the lowest isotherm $T^* = 0.7$ decrease with density. However, the three data of this isotherm lie in the metastable region, so that it cannot be conclusively decided wether the density dependence of the simulation data on this isotherm is physically correct.

The comparison shows that the behavior of the bulk viscosity of the Lennard-Jones model fluid in the liquid region agrees qualitatively with that found for liquid argon. Particularly, the enhancement of the bulk viscosity close to the critical point is also observed for argon on the liquid isotherms close to the critical temperature.

VI. PRESSURE-FLUCTUATION AUTOCORRELATION FUNCTIONS

In the Green-Kubo integral representation, the bulk viscosity is determined by the time integral of the pressure fluctuation autocorrelation function. Therefore, the temperature and density dependence of the bulk viscosity can be interpreted in terms of the decay behavior of the pressure-fluctuation autocorrelation functions. The state points for which the pressure autocorrelation function will be discussed are the same as those considered in Papers I and II for the shear-stress and velocity correlation functions. For the following discussion, it is interesting to compare the reduced Lennard-Jones time scale with a time scale corresponding to a real fluid. To represent the properties of the noble gas argon, the potential parameters $\sigma = 3.405 \times 10^{-10}$ m and $\varepsilon/k = 119.8$ K are often employed.[23] With these parameters, one reduced time unit corresponds to about 0.34 ps real time.

In Fig. 8, the short-time behavior of the pressure-fluctuation autocorrelation function at low gaseous densities is shown for three states on the lowest isotherm $T^* = 0.7$ and for six states along the isochor $\rho^* = 0.025$. The decay behavior of the autocorrelation function closely resembles that of the potential-potential shear-stress correlation function. At short times, the autocorrelation function decays rapidly to negative values, exhibits a minimum, then increases to reach a maximum and approaches the time axis from above. At low temperatures the minimum is followed by several oscillations, as the time integrals of the autocorrelation functions clearly reveal. With increasing temperature, the effect becomes smaller, and it vanishes at the highest displayed temperatures. The same effect was already observed in Papers I and II for the three contributions to the shear-stress correlation functions and the velocity autocorrelation functions and interpreted by the formation of bound states at low temperatures. The oscillations in the pressure-fluctuation autocorrelation functions are also caused by the formation of bound states. Moreover, this effect influences the initial slope of the bulk viscosity isotherms, e.g., the second bulk viscosity virial coefficient, yielding a nonzero contribution. Thus, the formation of bound states is partly responsible for the nonzero initial slopes of the bulk viscosity isotherms.

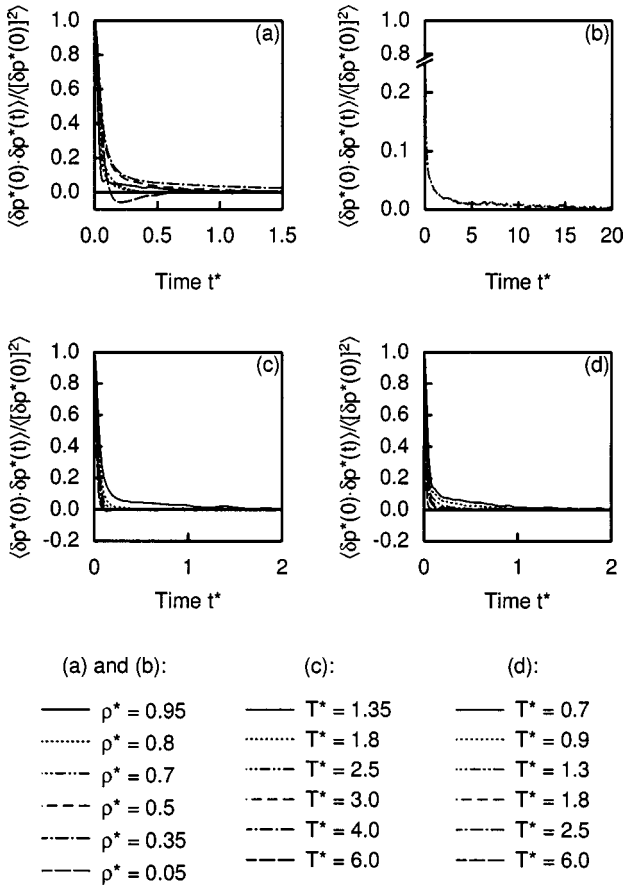

FIG. 9. Dependence of the normalized pressure-fluctuation autocorrelation function on density and temperature. Note the different abscissa scale in the subfigures. (a) and (b): on the supercritical isotherm $T^*=1.35$ close to the critical temperature. (c): along the isochor $\rho^*=0.3$ close to the critical density. (d) along the liquid isochor $\rho^*=0.85$.

Figure 9 depicts the pressure fluctuation autocorrelation function for selected state points on the near-critical isotherm $T^*=1.35$ and along the two isochors $\rho^*=0.3$ and 0.85. On the isotherm $T^*=1.35$ at the highest density near the freezing line, the autocorrelation function shows a rapid decrease at short times that suddenly becomes flatter at about $t^*=0.1$. At the transition between the two characteristic regions, small oscillations are observed. This behavior differs from that of the shear-stress correlation functions, which decay monotonically at high densities (see Paper I). At lower, but still liquid densities, the pressure-fluctuation autocorrelation function decays much faster at long times. At gaseous states, the decay of the autocorrelation function is similar to that of the potential-potential shear-stress correlation function as described above. In all these cases, the autocorrelation function has decayed to zero within a few reduced time units. Close to the critical density, the decay is much slower: Even within 20 reduced time units the pressure fluctuation autocorrelation function has not reached zero. Hence, the enhancement of the bulk viscosity in the vicinity of the critical point is caused by extremely slowly decaying pressure fluctuations.

On both isochors $\rho^*=0.3$ and 0.85, the decay of the pressure-fluctuation autocorrelation function becomes faster with increasing temperature. At the highest temperatures, the autocorrelation function has rapidly decayed to zero within less than 0.1 reduced time unit at both densities. The slowest decay is again observed close to critical point on the isochor $\rho^*=0.3$. At the liquid density $\rho^*=0.85$, the decay in the intermediate time regime at the lowest temperatures is similar to that of the potential-potential shear-stress correlation functions in this state region.

VII. CONCLUSIONS

In this work, the bulk viscosity of the Lennard-Jones model fluid was determined by equilibrium molecular-dynamics simulations using the Einstein relation method. About 350 simulated state points cover a large part of the fluid region from the low-density gas to the compressed liquid close to the freezing line in the temperature range between $T^*=0.7$ close to the triple-point temperature to $T^*=6.0$ (about 4.5 times the critical temperature). The uncertainty of the data is estimated to be 5%, increasing up to 30% at low-density gaseous states and in the vicinity of the critical point. With this comprehensive data set, the temperature and density dependences of the bulk viscosity were characterized. In the supercritical region, a large enhancement was found similar to that known for the thermal conductivity. However, the observed enhancement for the bulk viscosity extends over a much wider range of fluid states and is even observed at 4.5 times the critical temperature. This previously unexplored behavior of the bulk viscosity can be interpreted in terms of pressure-fluctuation autocorrelation functions. It turns out that the enhancement is caused by extremely slowly decaying pressure fluctuations in this state region. Often, the bulk viscosity is compared with the viscosity. However, the results of this work show that the bulk viscosity behaves completely differently than the viscosity throughout the fluid region. Also, with these results the bulk viscosity of the Lennard-Jones model fluid is better known than that of any real fluid.

ACKNOWLEDGMENTS

K.M. acknowledges an appointment as a guest researcher at the Physical and Chemical Properties Division of the National Institute of Standards and Technology in Boulder during summer 1999, where parts of this research were carried out. Computational resources for this work were provided by the Regional Computing Center for Lower Saxony at the University of Hannover (RRZN), the Konrad-Zuse-Zentrum for Information Technology in Berlin, and the NIST Information Technology Laboratory in Gaithersburg. The authors acknowledge the assistance of Dr. Simone Knief and Jürgen Fischer (RRZN) with the parallelization of the software, and the assistance of Denis Lehane at NIST.

[1] K. Meier, A. Laesecke, and S. Kabelac, Int. J. Thermophys. **22**, 161 (2001).
[2] K. Meier, *Computer Simulation and Interpretation of the Transport Coefficients of the Lennard-Jones Model Fluid* (Shaker, Aachen, 2002).
[3] K. Meier, A. Laesecke, and S. Kabelac, J. Chem. Phys. **121**, 3671 (2004).
[4] K. Meier, A. Laesecke, and S. Kabelac, J. Chem. Phys. **121**, 9526 (2004).
[5] K. Meier, A. Laesecke, and S. Kabelac (unpublished).
[6] J. O. Hirschfelder, C. F. Curtiss, and R. B. Bird, *Molecular Theory of Gases and Liquids* (Wiley, New York, 1954).

[7] H. J. M. Hanley and E. G. D. Cohen, Physica A **83**, 215 (1976).
[8] R. E. Graves and B. M. Argrow, J. Thermophys. Heat Transfer **13**, 337 (1999).
[9] R. Zwanzig, Annu. Rev. Phys. Chem. **16**, 67 (1965).
[10] E. Helfand, Phys. Rev. **119**, 1 (1960).
[11] M. P. Allen and D. J. Tildesley, *Computer Simulation of Liquids* (Clarendon, Oxford, 1987).
[12] R. Friedberg and J. E. Cameron, J. Chem. Phys. **52**, 6049 (1970).
[13] D. Levesque and L. Verlet, Mol. Phys. **61**, 143 (1987).
[14] C. Hoheisel, R. Vogelsang, and M. Schoen, J. Chem. Phys. **87**, 7195 (1987).
[15] M. Schoen, Dr. rer. nat.-Thesis, Abteilung für Chemie, Ruhr-Universität Bochum, 1986.
[16] D. Levesque, L. Verlet, and J. Kürkijarvi, Phys. Rev. A **7**, 1690 (1973).
[17] W. G. Hoover, D. J. Evans, R. B. Hickman, A. J. C. Ladd, W. T. Ashurst, and B. Moran, Phys. Rev. A **22**, 1690 (1980).
[18] D. M. Heyes, J. Chem. Soc., Faraday Trans. 2 **80**, 1363 (1984).
[19] D. M. Heyes, Can. J. Phys. **64**, 773 (1986).
[20] C. Hoheisel, J. Chem. Phys. **86**, 2328 (1987).
[21] See EPAPS Document No. E-JCPSA6-122-502501 for text files with tabulated simulation results and larger colored figures of this arcticle. A direct link to this document may be found in the online article's HTML reference section. The document may also be reached via the EPAPS homepage (http://www.aip.org/pubservs/epaps.html) or from ftp.aip.org in the directory /epaps/. See the EPAPS homepage for more information.
[22] ftp://FTP.Boulder.NIST.Gov/pub/fluids/Lennard-Jones
[23] P. Borgelt, C. Hoheisel, and G. Stell, Phys. Rev. A **42**, 789 (1990).
[24] M. Canales and J. A. Padró, Phys. Rev. E **60**, 551 (1999).
[25] D. M. Heyes, J. G. Powles, and J. C. Gil Montero, Mol. Phys. **78**, 229 (1993).
[26] A. Michels, J. V. Sengers, and P. S. van der Gulik, Physica (Amsterdam) **28**, 1216 (1962).
[27] B. W. Tiesinga, E. P. Sakonidou, H. R. van den Berg, J. Luettmer-Strathmann, and J. V. Sengers, J. Chem. Phys. **101**, 6944 (1994).
[28] J. V. Sengers and J. Luettmer-Strathmann, in *Transport Properties of Fluids. Their Correlation, Prediction and Estimation*, edited by J. Millat, J. H. Dymond, and C. A. N. de Castro (Cambridge University Press, Cambridge, 1996), pp. 113–137.
[29] D. K. Hoffman and C. F. Curtiss, Phys. Fluids **7**, 1887 (1964); **8**, 667 (1965); **8**, 890 (1965); C. F. Curtiss, M. B. McElroy, and D. K. Hoffman, Int. J. Eng. Sci. **3**, 269 (1965); D. E. Bennett and C. F. Curtiss, J. Chem. Phys. **51**, 2811 (1969).
[30] J. C. Rainwater, J. Chem. Phys. **81**, 495 (1984); D. G. Friend and J. C. Rainwater, Chem. Phys. Lett. **107**, 590 (1984); J. C. Rainwater and D. G. Friend, Phys. Rev. A **36**, 4062 (1987).
[31] J. A. Cowan and R. N. Ball, Can. J. Phys. **50**, 1881 (1972).
[32] D. G. Naugle, J. Chem. Phys. **44**, 741 (1966); D. G. Naugle, J. H. Lunsford, and J. R. Singer, *ibid.* **45**, 4669 (1966); W. M. Madigosky, *ibid.* **46**, 4441 (1967); D. S. Swyt, J. F. Havlice, and E. F. Carome, *ibid.* **47**, 1199 (1967).